

Medawar et al 2018 - Revision

1 **Effects of rising amyloid β levels on hippocampal synaptic**
2 **transmission, microglial response and cognition in *APP^{Swe}/PSEN1^{M146V}***
3 **transgenic mice**

4
5 **Ms Evelyn Medawar MSc* (medawar@cbs.mpg.de)**

6 **Dr Tiffanie Benway PhD* (tiffanie.benway@smallpharma.co.uk)**

7 **Dr Wenfei Liu PhD* (wenfei.liu.10@ucl.ac.uk)**

8 **Mr Taylor A. Hanan MSc (taylor.a.hanan@gmail.com)**

9 **Dr Peter Haslehurst PhD (peter.haslehurst@pharm.ox.ac.uk)**

10 **Dr Owain T. James PhD (owain.t.james@gmail.com)**

11 **Mr Kenrick Yap, MSc (kenrkyap@gmail.com)**

12 **Dr Laurenz Muessig PhD (l.mussig@ucl.ac.uk)**

13 **Ms Fabia Moroni MSc (fabia.moroni@gmail.com)**

14 **Dr Muzzamil A. Nahaboo Solim, MSBS (muzammil.solim.09@ucl.ac.uk)**

15 **Ms Gaukhar Baidildinova MSc (baidildag@mail.ru)**

16 **Ms Rui Wang (r.wang@ucl.ac.uk)**

17 **Dr Jill C. Richardson PhD^s (jillyrichardson@ntlworld.com)**

18 **Dr Francesca Cacucci PhD (f.cacucci@ucl.ac.uk)**

19 **Dr Dervis A. Salih PhD (dervis.salih@ucl.ac.uk)**

20 **Dr Damian M. Cummings PhD[†] (d.cummings@ucl.ac.uk)**

21 **Prof Frances A. Edwards PhD[†] (f.a.edwards@ucl.ac.uk)**

22

23 ***Joint first authors**

24 **†Joint corresponding authors**

25

26 **University College London, Gower Street, London, WC1E 6BT, UK**

27 **§ Neurosciences Therapeutic Area, GlaxoSmithKline R&D, Gunnels Wood Road,**

28 **Stevenage, SG1 2NY, UK**

Medawar et al 2018 - Revision

29 **Abstract**

30 **Background**

31 Progression of Alzheimer's disease is thought initially to depend on rising amyloid β and
32 its synaptic interactions. Transgenic mice (TASTPM; *APP*_{Swe}/*PSEN1*_{M146V}) show altered
33 synaptic transmission, compatible with increased physiological function of amyloid β ,
34 before plaques are detected. Recently, the importance of microglia has become apparent
35 in the human disease. Similarly, TASTPM show a close association of plaque load with
36 upregulated microglial genes.

37

38 **Methods**

39 CA1 Synaptic transmission and plasticity were investigated using *in vitro*
40 electrophysiology. Microglial relationship to plaques was examined with
41 immunohistochemistry. Behaviour was assessed with a forced-alternation T-maze, open
42 field, light/dark box and elevated plus maze.

43

44 **Findings**

45 The most striking finding is the increase in microglial numbers in TASTPM, which, like
46 synaptic changes, begins before plaques are detected. Further increases and a reactive
47 phenotype occur later, concurrent with development of larger plaques. Long-term
48 potentiation is initially enhanced at pre-plaque stages but decrements with the initial
49 appearance of plaques. Finally, despite altered plasticity, TASTPM have little cognitive
50 deficit, even with a heavy plaque load, although they show altered non-cognitive
51 behaviours.

52

53 **Interpretation**

54 The pre-plaque synaptic changes and microglial proliferation are presumably related to
55 low, non-toxic amyloid β levels in the general neuropil and not directly associated with
56 plaques. However, as plaques grow, microglia proliferate further, clustering around
57 plaques and becoming phagocytic. Like in humans, even when plaque load is heavy,
58 without development of neurofibrillary tangles and neurodegeneration, these
59 alterations do not result in cognitive deficits. Behaviours are seen that could be
60 consistent with pre-diagnosis changes in the human condition.

61

Medawar et al 2018 - Revision

62 **Funding**

63 GlaxoSmithKline; BBSRC; UCL; ARUK; MRC.

64

65 **Keywords**

66 Alzheimer's disease; dementia; mouse model; synaptic transmission; microglia; plaque;
67 neurodegeneration.

68

69 **Research in context**

70 *Evidence before this study*

71 There is a large body of research examining many aspects of phenotypes associated with
72 mouse models of Alzheimer's disease – a PubMed search for the terms Alzheimer* AND
73 mouse returns in excess of 21000 articles. However, there are few systematic articles
74 pulling together pathological, functional (electrophysiological), and behavioural
75 analyses across the life-span of such models. There is also a number of conflicting
76 outcomes, for example reports of impaired versus enhanced synaptic plasticity;
77 cognitive impairments or not.

78

79 Recently, the importance of microglia in Alzheimer's disease has come to the fore in
80 human Genome Wide Association Studies (GWAS), with variants of a number of
81 microglial genes identified as risk-factors for developing the disease. Interestingly, we
82 have recently reported that *Trem2* and other genes identified as risk-factors in humans
83 are strongly up regulated in close association to plaque development in the mouse
84 model used in this study. Moreover, this previous study predicted two of the most
85 recently identified genes that were identified in GWAS since the publication of our
86 paper.

87

88 We have previously used this model to identify the earliest synaptic changes and shown
89 changes in release of glutamate, the primary excitatory neurotransmitter in the brain, to
90 occur even before plaques are detectable.

91

92 *Added value of this study*

93 By studying this transgenic mouse model of Alzheimer's disease, throughout the
94 development of plaques, from prior to detection through to heavy plaque loads, we have

Medawar et al 2018 - Revision

95 been able to identify a clear time course of key phenotypic changes associated with early
96 disease. In particular, this study identifies the very early changes in microglia and can
97 separate the time course of the microglial phenotype. In addition, we detail the changes
98 in synaptic plasticity over time and importantly identify that, like in humans in the
99 absence of Tau tangles or neurodegeneration, considerable synaptic changes can occur
100 and a heavy plaque load without resulting in substantial cognitive loss.

101

102 *Implications of all the available evidence*

103 Our data indicate that rising amyloid beta prior to detectable plaque deposition results
104 in changes in synaptic function that likely reflects an enhanced physiological effect of
105 amyloid beta. At this stage, microglia proliferate but do not activate. Once plaques begin
106 to appear, microglia migrate to surround the plaque and become phagocytic, likely
107 targeting dystrophic synapses and neurites caused by the cloud of highly-toxic amyloid
108 beta around the plaque. Similarly to humans, who have plaques but no tangles and have
109 yet to develop substantial neurodegeneration, cognitive deficits are not seen, even with
110 a heavy plaque load; behavioural changes are limited to anxiety-like effects.

111

112 This investigation of the parallel time-course of events highlights the probability that, if
113 progression of disease can be reversed or slowed early enough, before Tau tangles and
114 substantial neurodegeneration occur, the symptoms of cognitive decline could be very
115 largely avoided. Moreover, it suggests that the substantial increases in microglia number
116 and upregulation of their specific gene expression in association with plaques, is not
117 associated with cognitive loss and may indeed be protective.

118 **Introduction**

119 The onset and progression of Alzheimer's disease (AD) is most likely initiated by
120 environmental factors interacting with predisposed genetic risks, many of which have
121 now been identified in genome-wide association studies (see reference 1 for review). In
122 familial AD, an inherited mutation causes rising amyloid β ($A\beta$) levels and it has long
123 been established that this triggers a chain of events that leads to the eventual cognitive
124 decline.^[2] In sporadic AD, it is highly likely that initial triggering events (genetic and/or
125 environmental) also lead to rising $A\beta$ and that, like in the familial disease, $A\beta$ levels
126 represent an essential contributor to the ongoing pathology and eventual
127 neurodegeneration.^[3, 4] Under normal physiological conditions, $A\beta$ acts as an activity-
128 dependent synaptic modulator which, when released from presynaptic neuronal
129 terminals, increases probability of glutamate release.^[5] Inappropriate neuronal activity
130 and/or genetic imbalances in production versus clearance mechanisms may thus lead to
131 a prolonged rise in $A\beta$ levels,^[6] enabling the formation of $A\beta$ oligomers and deposition of
132 plaques. It is notable that restoring γ -frequency oscillations in transgenic mouse models
133 expressing genes harbouring familial mutations associated with familial AD, reduces $A\beta$
134 load^[7] and restores cognitive deficits.^[8]

135
136 Animal models for AD have generally depended on transgenic expression, or more
137 recently knock-in of the gene variants that cause the familial dominantly inherited forms
138 of the disease, particularly amyloid precursor protein (*APP*) or presenilin 1 or 2 (*PSEN1*
139 or *PSEN2*). This is an effective approach for initiating the rise in $A\beta$ and the deposition of
140 plaques, albeit by a different trigger than in sporadic AD. According to the 'amyloid
141 hypothesis', in the human disease, rise in $A\beta$ and plaque deposition is suggested to lead
142 to altered neuronal ionic homeostasis and increased oxidative stress. Together, these
143 may result in increased kinase activity on microtubule-associated protein Tau, resulting
144 in Tau hyperphosphorylation and neurofibrillary tangle formation.^[9] The exact
145 mechanisms linking $A\beta$ and Tau phosphorylation remain unclear and unfortunately,
146 despite the initiation of $A\beta$ pathology, mouse models with genes for familial Alzheimer's
147 disease do not completely recapitulate these later events. As documented in the initial
148 descriptions of the TASTPM mice, which are hemizygous for both human APP_{Swe} and
149 human $PSEN1_{M146V}$, plaques are first detected at approximately 4 months of age and a
150 considerable plaque load develops by 8 months.^[10, 11] Furthermore, phosphorylation of

Medawar et al 2018 - Revision

151 Tau is detectable in the dystrophic neurites around plaques,^[11] recently suggested to be
152 an early stage of Tau pathology.^[12] An inability to extinguish hippocampal-dependent
153 contextual fear conditioning at 4 months when plaques are first detected^[13, 14] and a
154 deficit in novel object recognition at 6 months,^[15] have also been reported.

155
156 We recently reported alterations in synaptic transmission preceding the detection of
157 plaques, manifesting as a loss of spontaneous action potentials in Schaffer collateral
158 axons and a concomitant increase in probability of glutamate release.^[16] Importantly, we
159 have demonstrated an almost 1:1 correlation of plaque load with expression of a module
160 of microglial genes throughout the life of these and other transgenic mice. This
161 correlation in A β mice contrasts with the interaction of microglia and neurofibrillary
162 tangles in mice with Tau mutations, in which microglial genes are only upregulated with
163 advanced tangle load (www.mouseac.org).^[10]

164
165 Here we extend our previous studies on TASTPM mice to understand the relationship
166 between early changes in synaptic transmission, synaptic plasticity, cognitive function
167 and microglia. We study the development of plaques in more detail and dissect out the
168 microglial response to distinguish between the numbers of microglia and their
169 phagocytic status. We find that, like synaptic changes, microglia are more prevalent even
170 before plaques are detectable, whereas their phagocytic phenotype is age-related,
171 coming much later. We then proceed to study hippocampal synaptic plasticity and
172 hippocampus-dependent learning, in the forced-alternation T-maze, enabling
173 identification of A β phenotypes, finding little cognitive deficit even with a heavy plaque
174 load but clear behavioural changes, probably related to increased levels of anxiety.
175 While we continue to focus mainly on the previously defined TASTPM mice (double
176 hemizygote), we have broadened the study to investigate dose dependency of the
177 transgene by including mice homozygous for both genes. The effect of the individual
178 genes is also investigated in mice with hemizygous expression of only one or the other
179 gene. When not otherwise defined, TASTPM mice hence refers to the double hemizygous
180 mouse.

Medawar et al 2018 - Revision

181 **Methods**

182 *Animals*

183 All experiments were performed in agreement with the UK Animals (Scientific
184 Procedures) Act 1986, with local ethical approval and in agreement with the
185 GlaxoSmithKline statement on use of animals. Male TASTPM mice and C57Bl/6j mice
186 were supplied by GlaxoSmithKline and bred either at Charles River Laboratories
187 International, Inc. (Margate, UK) or at UCL by crossing male homozygous TASTPM with
188 female C57Bl/6j. Age-matched, non-littermate male C57Bl/6j mice were used as wild
189 type controls. In some experiments, double homozygous TASTPM were bred. Single
190 mutant TAS (APP_{Swe})^[17] or TPM ($PSEN1_{M146V}$)^[15] mice were bred by crossing
191 hemizygous parents. Mice from Charles River were shipped to UCL upon weaning at 21-
192 days-old.

193
194 In this study we avoided single housing by keeping mice in large open cages (20 x 35 x
195 45 cm) and enriching their environments. Under these conditions, while the aggressive
196 nature of the TASTPM mouse is not completely avoided, it is less of a problem and
197 allows group housing to be maintained over the lifetime of the mice. Thus, cages
198 containing 2-8 male mice were maintained in a 12-hour light/12-hour dark cycle with
199 food (Envigo 2018 Teklad global 18% protein rodent diet) and water *ad libitum*.
200 Environmental enrichment consisted of changes of food location, bedding type (e.g.
201 tissue, shredded paper, paper roll, paper bags) and inanimate objects (e.g. running
202 wheels, rodent balls, tubing, houses (mostly purchased from Eli Lilly Holdings Limited,
203 Basingstoke, UK)) within the cage at least once per week. Mice were used for
204 experimentation at the ages stated (\pm 0.5 months) and, where unavoidable, were single-
205 housed for no longer than 24 hours. Tails or ear punches were used for genotyping by
206 standard PCR protocols to ensure the presence of the expected genes.

207

208 **Genotyping**

209 *Genotype confirmation using conventional PCR methods*

210 Briefly, genomic DNA was extracted using the 'HotSHOT' lysis method. Alkaline lysis
211 reagent (25 mM NaOH, 0.2 mM EDTA, pH12) was added to tissue samples prior to
212 heating to 95°C for 30 minutes. The sample was then cooled to 4°C before the addition of

Medawar et al 2018 - Revision

213 neutralisation buffer (40 mM Tris-HCl, pH 5). The PCR reaction was performed through
214 addition of MyTaq DNA Polymerase (Bioline) reaction buffer and primer pairs:

215

216 TAS (APP_{Swe}):

217 5' GAATTGACAAGTTCCGAGGG 3'

218 5' GGGTACTGGCTGCTGTTGTAG 3'

219

220 TPM (PSEN1_{M146V}):

221 5' GTTACCTGCACCGTTGTCCT 3'

222 5' GCTCCTGCCGTTCTCTATTG 3'

223

224 using the cycling parameters: 94°C (30 s), 58°C (30 s), 72°C (30 s), for 30 cycles and a
225 final extension at 72°C for 4 min. PCR product sizes 366 bp for TAS and 104 bp for TPM.

226

227 **Immunohistochemistry**

228 Animals were deeply anaesthetised (1:10 Euthatal:Intra-Epicaine, National Veterinary
229 Supplies) and transcardially perfused with 0.1 M phosphate buffer saline (PBS) followed
230 by 10% buffered formal saline (Pioneer Research Chemicals Ltd). Alternatively, single
231 hemispheres were drop-fixed immediately following brain extraction for
232 electrophysiology. The brains were post-fixed in 10% buffered formal saline for 24hrs
233 and cryoprotected in 30% sucrose/0.03% sodium azide/PBS at 4°C for at least 24hrs
234 before sectioning or storage. Transverse sections were cut at 30 µm through the full left
235 hippocampus using a frozen sledge microtome (SM 2000 R, Leica) and collected into a
236 24-well plate containing PBS/sodium azide (0.03%) for storage at 4°C. Serial sections
237 were placed in separate wells until all wells contained a section and collection then
238 continued serially from Well 1 so that within each well the transverse sections were
239 from the length of the hippocampus at least 720µm apart.

240

241 Standard immunohistochemical techniques were employed. For Aβ staining only,
242 antigen retrieval was achieved by submerging sections in 10 mM sodium citrate (pH 6.0)
243 in 0.05% Triton X-100 and heated in a water bath at 80°C for 30 minutes. Sections for all
244 immunohistochemistry were then washed in PBS, followed by 0.3% Triton X-100 in PBS
245 and subsequent blocking in 8% horse serum/Triton/PBS for 1 hour. Incubation with

Medawar et al 2018 - Revision

246 primary antibody (table 1) in blocking solution was performed overnight at 4°C.
247 Sections were again washed with Triton/PBS. The appropriate Alexa-conjugated
248 secondary antibody (1:500; Invitrogen) was added to blocking solution for a 2-hour
249 incubation at room temperature in the dark. Following PBS wash, DAPI (1:10,000) was
250 applied to all sections for 5 minutes. Sections were washed for a final time in PBS before
251 mounting. Age-matched sections from wild type controls were stained in parallel for all
252 ages. Sections were mounted in anatomical order onto SuperFrost Plus glass slides by
253 floating on PBS and then cover-slipped using Fluoromount G mounting medium.

254

255 *Imaging and data analysis*

256 Sections were imaged for quantification using an EVOS FL Auto Cell Imaging System
257 (Life technologies). Tiled images were taken of the whole transverse hippocampal
258 section using a 20X objective. To determine cell densities, an area of 400 µm x 240 µm
259 was defined in the CA1, CA3 and the inner blade of the dentate gyrus. Cell counts were
260 performed using Adobe Photoshop CS6. A minimum of three sections were used to
261 create a mean for each animal. Sections for any given condition were obtained from the
262 same collection well within the 24-well plate and were therefore a minimum of 720 µm
263 apart, thus avoiding multiple counts of the same cells. Counts of objects touching the
264 boundaries of the area of interests were only included from the north and east borders
265 and excluded from the south and west borders.

266

267 **Electrophysiological recordings**

268 *Acute hippocampal brain slice preparation*

269 Mice were decapitated and the brain rapidly removed and placed in ice-cold dissection
270 artificial cerebrospinal fluid (ACSF, containing (in mM): 125 NaCl, 2.4 KCl, 26 NaHCO₃,
271 1.4 NaH₂PO₄, 20 D-glucose, 3 MgCl₂, 0.5 CaCl₂, pH 7.4, ~315 mOsm/l). After
272 approximately two minutes in ice-cold dissection ACSF, the brain was prepared for
273 slicing by removing the cerebellum, hemisection of the forebrain and a segment cut
274 away from the dorsal aspect of each hemisphere at an angle of approximately 110° from
275 the midline surface to optimise slicing transverse to the hippocampus. Each hemisphere
276 was then glued with cyanoacrylate (Loctite 406, Henkel Loctite Limited, UK) on this
277 surface onto the stage of a vibrating microtome (Integraslice model 7550 MM, Campden
278 Instruments, Loughborough, UK) containing frozen dissection ACSF and 400 µm

Medawar et al 2018 - Revision

279 transverse slices of hippocampus cut. As each slice of a hemisphere was cut, the
280 hippocampus was dissected out, retaining a portion of entorhinal cortex and the
281 resulting smaller slice was placed into a chamber containing 'Carbogenated' (95%
282 O₂/5% CO₂; BOC Limited) dissection ACSF at room temperature (approximately 21°C).
283 After 5 minutes, slices were then transferred into a fresh chamber held at 36°C with the
284 same dissection ACSF. At 5-minute intervals, they were then consecutively transferred
285 to physiological Ca²⁺ and Mg²⁺ ion concentrations (in mM): i) 1 Mg²⁺, 0.5 Ca²⁺; ii) 1 Mg²⁺,
286 1 Ca²⁺; iii) 1Mg²⁺, 2 Ca²⁺. After approximately 20 minutes at 35°C (i.e., once transferred
287 into the 1 Mg²⁺, 2 Ca²⁺ ACSF).

288

289 *Patch-clamp recordings in brain slices*

290 Once transferred to 1 Mg²⁺, 2 Ca²⁺ ACSF, slices were allowed to return to room
291 temperature and after at least a further 40 minutes recovery time, a single slice was
292 transferred to a submerged chamber and superfused with recording ACSF (containing
293 (in mM): 125 NaCl, 2.4 KCl, 26 NaHCO₃, 1.4 NaH₂PO₄, 20 D-glucose, 1 MgCl₂, 2 CaCl₂,
294 bubbled with Carbogen). Individual CA1 pyramidal or dentate gyrus granule neurones
295 were visualised using infrared-differential interference contrast microscopy on an
296 upright microscope (model BX50WI, Olympus, UK). Glass microelectrodes for patch-
297 clamp were pulled from borosilicate glass capillaries (Catalogue number GC150F-7.5,
298 1.5 mm OD x 0.86 mm ID, Biochrom-Harvard Apparatus Ltd, Cambridge, UK) on a
299 vertical puller (model PP830, Narishige International Ltd, London UK). Electrodes (tip
300 resistance approximately 5 MΩ) were filled with a CsCl-based internal solution
301 (containing (in mM): CsCl 140, HEPES 5, EGTA 10, Mg-ATP 2, pH 7.4, ~290 mOsm/l).
302 Patch-clamp recordings were performed using an Axopatch 1D (Molecular Devices,
303 Sunyvale, CA, USA), and current signals low-pass filtered at 10 kHz then 2 kHz
304 (Brownlee Precision Model 440, NeuroPhase, Santa Clara, CA, USA) during digitization
305 (10 kHz; 1401plus, Cambridge Electronic Design, Limited, Cambridge, UK) and acquired
306 using WinWCP (for isolated events; version 4.6.1; John Dempster, Strathclyde
307 University, UK) and WinEDR (for continuous recordings; John Dempster, Strathclyde
308 University, UK). Stimulation was applied *via* a patch electrode filled with ACSF, placed
309 extracellularly in the appropriate axon path using a square pulse constant-voltage
310 stimulator (100 μs; DS2A-MkII, Digitimer Ltd, UK) triggered by WinWCP.

311

Medawar et al 2018 - Revision

312 WinEDR synaptic analysis software was used for detection of spontaneous and
313 miniature currents and WinWCP used to analyse identified spontaneous, miniature and
314 evoked currents. Criteria for detection of spontaneous or miniature currents was to
315 remain over a threshold of 3 pA for 2 ms. Currents were inspected by eye and only
316 included if the rise time was <3 ms and faster than the decay.

317

318 *Field potential recordings in brain slices*

319 Slices were transferred as needed to a heated ($30\pm 1^\circ\text{C}$) submerged chamber and
320 superfused with ACSF and allowed to recover for 1 h in the recording chamber. A glass
321 stimulating electrode (filled with ACSF, resistance $\sim 2\text{ M}\Omega$) and an identical recording
322 electrode (connected to an AxoClamp 1B via a 1X gain headstage) were both positioned
323 in stratum radiatum of the CA1 field to obtain a dendritic excitatory postsynaptic field
324 potential (fEPSP). Recordings were controlled and recorded using WinWCP software (as
325 above), filtered at 10 kHz and subsequently at 3 kHz and digitized at 10 kHz via a
326 micro1401 interface (Cambridge Electrical Designs, UK). Stimuli (constant voltage 10-
327 70V, 100 μs ; model Digitimer DS2A-MkII or Grass SD9) were applied at 0.1 Hz and
328 resultant fEPSPs subsequently averaged over consecutive 1-minute intervals.
329 Stimulation intensity was set at approximately 30-50% of the intensity required to
330 evoke a population spike or the maximum fEPSP amplitude obtained and a ≥ 15 -minute
331 stable baseline recorded. LTP conditioning was applied at test-pulse stimulus intensity
332 and consisted of either 3 trains of tetani, each consisting of 20 pulses at 100 Hz, 1.5 s
333 inter-train interval or 4 trains of theta-burst stimuli (TBS), each train consisting of 4
334 pulses at 100 Hz repeated 8 times at 20 Hz; inter-train interval 1 minute. Following
335 conditioning, fEPSPs were evoked at 0.1 Hz for 1 hour.

336

337 **Behavioural testing**

338 *T-maze forced alternation task*

339 Previously reported methods, optimised for mouse, were used to assess hippocampus-
340 dependent learning [18]. Mice were food deprived to 90% free-feeding-weight, beginning
341 2 days before the start of the habituation phase and with *ad libitum* access to water.
342 Each mouse was handled at the start of food deprivation and throughout T-maze
343 habituation for 15-20 minutes per weekday.

344

Medawar et al 2018 - Revision

345 The T-maze was constructed from three arms, each measuring 50 x 8 cm with 10 cm
346 colourless Perspex walls and a grey floor, mounted on a table in the centre of a room
347 with numerous distal visual cues, such as black and white posters on the walls. Black
348 barriers were used to block the start and goal arms. Reward consisted of a drop of Nestlé
349 Carnation™ condensed milk that was placed at the end of each goal arm. Arms were
350 cleaned with 70% ethanol between all runs to reduce odour cues. In addition, in an
351 inaccessible well a drop of reward is always present in both arms.

352
353 Mice received 4 days of habituation to the maze, during which time they were allowed to
354 explore the maze for 5 minutes with all arms open. During the first two days of
355 habituation, reward was scattered along the floor and in food wells to encourage
356 exploratory behaviour; then restricted to only the food wells at the ends of the goal arms
357 in the last two days.

358
359 The behavioural regime lasted for three weeks, with five days of training per week. Each
360 day, animals received six trials; each trial consisted of a sample and choice run. In the
361 sample run, one arm was blocked off. The mouse was placed at the starting point at the
362 base of the T, the barrier was removed and the mouse was allowed to go to the available
363 arm and given 20 s to eat a drop of reward from the food well. For the choice run, the
364 mouse was immediately returned to the starting point and the barrier in the previously
365 blocked arm removed. The starting barrier was then raised and the animal allowed to
366 choose between the two arms but only rewarded if it chose the previously unvisited
367 arm. Thus, a correct choice was scored when the mouse selected the arm not visited in
368 the sample run. After the choice run, the mouse was removed from the maze and placed
369 in its holding box. The location of the sample arm (left or right) was varied
370 pseudorandomly across the session and mice received three left and three right
371 presentations, with no more than two consecutive trials with the same sample location.
372 Animals were allowed a maximum of 5 minutes to make a choice to enter a goal arm in
373 both runs before a trial was aborted. If an incorrect arm was chosen during the choice
374 run, the mouse was confined in the arm with no reward for 20 s and then removed from
375 the maze.

376

Medawar et al 2018 - Revision

377 During the first two weeks of training the choice run followed immediately after the
378 sample (test) run (there was a delay of approximately 15 s between runs for cleaning
379 and resetting the maze). Data was analysed in blocks of 2 days and hence blocks 1-5
380 represent the first 2 weeks of training.

381
382 On the first day of the third week, mice received a repeat of the previous training
383 sessions in order to assess retention of the task (block 6). On the following four days,
384 longer delays (2-10 minutes) were introduced between the sample and choice runs to
385 extend the time that the previous choice was to be held in memory (blocks 7 and 8 in
386 response times). During these intervals, each animal was placed in a separate holding
387 box. Each mouse received two of each of the delay periods per day, varied
388 pseudorandomly both within and across days. Response times were calculated from the
389 time that the starting block was removed until the mouse made a choice of arms and all
390 four paws had crossed the entry point. Squads of 15-17 mice were run per day. During
391 training data are presented as blocks averaged across 2 days for each animal and
392 expressed as mean \pm SEM. For delays the four runs for each delay are averaged.

393
394 *Elevated plus maze*
395 The plus-maze was constructed from two enclosed arms (30 cm x 5 cm x 20 cm) and two
396 open arms (30 cm x 5 cm x 0.8 cm) connected by a small central platform (5 x 6 cm); the
397 two closed and two open arms were positioned opposite each other, respectively. The
398 maze was elevated 30 cm above a table.

399
400 Mice were placed in the centre of the plus maze facing an open arm and allowed to freely
401 explore the maze for one 6-minute trial. The time spent on each arm (open *versus*
402 closed) was recorded, as well as the number of entries into the arms. An entry into an
403 arm was defined as all four paws resting on a given arm.

404
405 *Open field*
406 The open field consisted of a plastic cylinder (diameter: 47.5 cm, height 36 cm) with a
407 white plastic floor. Mice were placed on the periphery of the open field floor and allowed
408 to explore freely for 30 minutes. The path of each mouse was recorded using dacQUSB
409 recording system (Axona, St. Albans, U.K) at a sample rate of 50 Hz. The open field was

Medawar et al 2018 - Revision

410 optically divided into a central circle and a peripheral ring, each with equal area. The
411 path of the mouse was analysed offline using ImageProPlus. Path length and dwell times
412 in the periphery and centre were calculated using custom made routines written in
413 Matlab R2010a (MathWorks).

414
415 *Light/dark box*
416 The dark box^[19] measured 20 cm x 20 cm x 30 cm, with black walls, floor and lid. The
417 light box measured 30 cm x 30 cm x 30 cm with a white floor and light grey walls. The
418 boxes were connected by an opening in the partition between the two compartments. An
419 overhead light provided bright illumination in the light box. Mice were placed in the
420 centre of the light compartment facing away from the opening and then allowed to
421 explore for a period of 6 minutes. Time spent in each box and the number of entries into
422 each box were recorded. An entry into a box was defined as all four paws resting inside
423 the given box.

424
425 **Statistics**
426 All data analysis was carried out blind to genotype. All statistics were performed using
427 Graphpad Prism 6 with appropriately designed two-tailed t-test or ANOVA. Post hoc
428 tests were only performed if a significant interaction between the independent variables
429 was obtained. Animals were considered as independent samples and, where multiple
430 data were collected from an animal, these were averaged (mean) prior to pooling. Thus
431 sample sizes represent the number of animals. Unless stated otherwise, data are
432 presented as mean \pm SEM and differences considered significant at $p < 0.05$.

433 **Results**

434 *Plaque development in hippocampus*

435 In TASTPM mice of different ages, individual plaques were counted in the hippocampus
436 and their sizes measured to assess whether the distribution changed over time (Fig 1).
437 Initially, at 3-4 months of age, only small plaques could be detected ($<100 \mu\text{m}^2$) and
438 these were very sparse (Fig. 1a-c). However, the number of small plaques increased
439 exponentially, initially approximately doubling every month, and continuing to increase
440 at a slower rate until 14 months of age (Fig. 1b). Hence, at least up until this age, new
441 plaques were being seeded. By 7 months plaques up to $200 \mu\text{m}^2$ were consistently seen
442 but were similar in frequency to the smallest plaques at 3-4 months, presumably
443 representing the growth of the earliest seeds. Plaques of $>500 \mu\text{m}^2$ were only
444 consistently detected at ages over 10 months but, from this age on, a wide range of
445 plaques sizes were evident, with occasional plaques of over $2500 \mu\text{m}^2$ detected.
446 Interestingly, between 14 and 15 months of age, very little change in the number of
447 plaques was detected but the largest plaques continued to grow. As individual plaques
448 were not tracked over time, we cannot be entirely sure that the progression up to 14
449 months is due to continuous seeding of small plaques that gradually grow with ongoing
450 plaque deposition; however, this seems the most likely explanation. The fact that the
451 rate of addition of small plaques decreases gradually until it plateaus around 14 months
452 of age suggests that, as the plaques get denser, some of the small plaques start to fuse
453 with larger plaques. In some cases, large plaques were present that possessed a halo of
454 $\text{A}\beta$ around the dense core, with dense puncta of $\text{A}\beta$ visible within the halo, possibly
455 representing more recently seeded plaques being engulfed as the large plaque grows
456 (Fig 1a).

457
458 When the gene-dose was doubled by using double homozygous TASTPM mice, plaques
459 were first detected at about 2 months of age (Fig 1e). Similarly to the hemizygous mice,
460 plaque density and size increased with age but perhaps surprisingly, did not reach a
461 greater density than that observed in the hemizygotes.

462
463 Mice carrying only the single mutations were also examined. In TAS mice (APP_{Swe}), small
464 plaques were detected at 16 months. While plaque density and size increased with age,
465 plaque loads did not reach that seen in the double mutant TASTPM mice, even at the

Medawar et al 2018 - Revision

466 very advanced age of 27 months. In TPM mice (PSEN1_{M146V}), there were no plaques
467 observed at any age.

468

469 *Microglia*

470 Having previously observed that a module of microglial genes increased in expression in
471 A β mice (including TASTPM) in close correlation with plaque load^[10], we went on to
472 examine the densities of total and CD68 positive of microglia in more detail in these
473 mice (Fig 2). There was an increased density of microglia (assessed by Iba1 positive
474 cells) in CA1 at very early ages, with increases (approximately double) compared to wild
475 type already evident by 2 months of age, even before plaques could be detected (Fig
476 2a&c; 2-8 months, n=6-12, two-way ANOVA, p<0.01). However, note that A β levels are
477 already raised by 2 months^[16] and it is possible that small plaque seeds (< the 10 μm^2
478 threshold) may already be depositing at this time. There was also an age-dependent
479 increase in Iba1 positive microglia in both wild type and TASTPM mice at around 10
480 months of age.

481

482 In contrast to total microglia, the microglial phagocytic phenotype, as measured by CD68
483 labelling, was very low in all young animals and only increased from around 10-12
484 months. Again, this happened in both wild type and TASTPM mice. The percentage of
485 phagocytic microglia tended to be slightly higher in TASTPM mice as compared to wild
486 type (14-20 months, n=5-9, two-way ANOVA p=0.07). This coincided with the
487 appearance of large plaques (Fig 1c&d). Interestingly, the number of microglia and their
488 CD68 status seem to plateau at this stage, with no further increase in density beyond 12
489 months of age.

490

491 When the double homozygous TASTPM mice were examined, a very similar pattern was
492 observed for densities of both total microglia and CD68 positive microglia (Fig 2d). As
493 expected both plaque load and microglial response was greater in the homozygous mice.

494

495 Sections from single mutant mice were also stained for both IBA1 and CD68. The APP_{Swe}
496 TAS mice, which develop plaques from around 16 months (Fig 1f), had a higher total and
497 CD68 positive microglia at both 18 and 27 months of age (main effects of genotype for
498 both Iba1 and CD68 in separate two-way ANOVAs; p<0.05). In contrast, the PSEN1_{M146V}

Medawar et al 2018 - Revision

499 TPM mice, which do not develop plaques at any age, showed no difference from wild
500 type mice in their microglial phenotype at 4 months of age for either total or CD68
501 positive microglia (Fig 2g, two-tailed t-test, $p>0.5$).

502
503 Very similar changes in total microglial and CD68 positive microglial densities were
504 found in dentate gyrus, CA3 and subiculum (data not shown).

505
506 *Synaptic currents in CA1 neurones*

507 Spontaneous excitatory activity

508 When spontaneous excitatory currents are recorded from CA1 pyramidal neurones in
509 the presence of a GABA_A receptor antagonist (gabazine, 6 μ M), the substantial loss of
510 spontaneous activity we have previously reported up to 4 months of age^[16] is largely
511 maintained through to 18 months (Fig 3a). At 8 months there was almost a complete
512 loss of action potential-dependent spontaneous activity in the transgenic mice (Fig 3aii),
513 with the frequency almost exactly the same as that of miniature currents (Fig 3aiii)
514 observed in the presence of 1 μ M tetrodotoxin. This result was almost identical to what
515 we have previously reported at 4 months. By 12-18 months, a decrement in frequency of
516 miniature EPSCs had also developed but the action potential mediated spontaneous
517 excitatory current frequency, although significantly lower in transgenic mice than wild
518 type mice, were at a higher frequency than the miniature currents in the same genotype,
519 implying that some spontaneous action potential-mediated activity was occurring in the
520 transgenic mice at these older ages (Fig 3a). There were no differences between
521 genotypes of mEPSC amplitudes or decay time constants (data not shown).

522
523 When excitatory activity was evoked by stimulating the Schaffer collaterals in slices
524 from older animals, the previously reported increase in release probability at 4 months,
525 as assessed by a lower paired-pulse facilitation and confirmed by a reduction in failure
526 to release glutamate in response to minimal stimulation^[16], was maintained. Thus, at 12
527 months of age, paired-pulse ratio was lower in TASTPM than wild type mice at both 25
528 and 50 ms inter-stimulus intervals ($n=5-8$, two-way ANOVA, main effect of genotype
529 $p<0.02$), while at 18 months of age, the lower paired-pulse ratio was only evident at 25
530 ms, resulting in a genotype x interval interaction ($p<0.05$) and a highly significant Sidak
531 post hoc pairwise comparison between genotype at 25 ms ($p<0.005$).

Medawar et al 2018 - Revision

532

533 Inhibitory activity is unchanged

534 Although we have concentrated our detailed analysis on glutamatergic activity, we were
535 able to gain an overview of inhibitory activity from the spontaneous activity recorded in
536 the absence of antagonists by utilising CsCl as the internal patch pipette solution. Hence,
537 in the experiments examining pharmacologically isolated EPSCs above, initially
538 spontaneous currents were recorded in the absence of receptor antagonists. When the
539 GABA_A receptor antagonist was included in the perfusion solution, the frequency of
540 currents was decreased to about 5-10% in wild type slices. Consequently, GABA_A
541 receptor-mediated activity contributes about 90% of the frequency of the initial
542 recording of mixed spontaneous activity. Note that, if the recording were made in the
543 presence of a glutamatergic antagonist, any currents that were due to spontaneous
544 glutamatergic activity mediating feed-forward or feed-back inhibition would be lost.
545 Hence, the assessment of the drug-free frequency is a better assessment of the
546 contribution of inhibition with the understanding that this will overestimate frequency
547 by about 10%. Under these conditions we find that there is no significant change in
548 inhibitory synaptic activity in TASTPM mice at any age from 4 to 18 months (Fig
549 3c). Note that, considering the very substantial change in spontaneous glutamatergic
550 activity, this implies that very little of the GABAergic activity is dependent on
551 glutamatergic input.

552

553 Synaptic plasticity is altered in TASTPM mice

554 Considering the changes in excitatory transmission it seemed likely that synaptic
555 plasticity, in particular, long-term potentiation (LTP), the best cellular model we have
556 for the laying down and retrieval of memory^[20], could be altered. To assess effects on
557 LTP, field potentials were recorded from CA3-CA1 synapses in acute brain slices
558 prepared from TASTPM mice at ages preceding detectable A β plaques (2 months)
559 through to ages with a heavy plaque load (12-18 months).

560

561 Field input-output relationship was not significantly changed at any of the ages tested
562 (Fig 4a). Moreover, unlike our previously reported result using patch clamp recording in
563 the presence of a GABA_A receptor antagonist^[16], in field recordings with the inhibitory
564 network intact, paired-pulse ratios were not significantly changed between genotypes at

Medawar et al 2018 - Revision

565 any of the ages tested (Fig 4b). This suggests that the observed changes in paired-pulse
566 ratio were masked when GABAergic activity was not blocked, presumably, at least in
567 part, by feed-forward inhibition decreasing release on the second stimulus.

568
569 At 2 months of age, LTP is altered in TASTPM mice but this is dependent on the
570 induction protocol. When LTP was induced by tetanic stimulation in these young mice,
571 the magnitude of LTP was greater in slices from TASTPM than from wild type mice.
572 Paired-pulse ratios remained unaltered when the last ten minutes of the post-induction
573 recordings was compared to the baseline in both genotypes (Fig 4c&d). This suggested
574 that the change in amplitude seen in LTP was due to a postsynaptic change. In contrast,
575 when LTP was induced using TBS, there was no difference between the wild type and
576 transgenic mice (Fig 4e). Surprisingly, however, despite LTP remaining unchanged after
577 theta burst stimulation, the paired-pulse ratio decreased significantly between the pre-
578 induction baseline and the last 10 minutes of LTP in the TASTPM but not in the wild type
579 mice. This suggests that the locus of expression of this form of LTP is likely to have a
580 presynaptic component in transgenic mice at this age. Note that, considering an increase
581 in release probability would be expected to enhance the postsynaptic response, this
582 would suggest that the postsynaptic contribution to LTP could be decreased in the
583 transgenic mice possibly with one locus of change compensating for the other.

584
585 At 4 months of age, the effects of the different stimulus protocols had changed. By this
586 age, a clear deficit was seen in LTP induced by tetanic stimulation, which was the
587 reverse change to that seen at 2 months. Moreover, similar effects were seen in two
588 separate cohorts of 4-month-old mice (cohort 1 shown in Fig 4c; pooled data shown in
589 Fig 4d.

590
591 TBS-induced LTP (Fig 4e) was, like at 2 months, of similar magnitude between
592 genotypes but analysis of paired-pulse ratios, following LTP induction, indicated that
593 LTP has a similar locus of expression in the two genotypes.

594
595 In addition, chemically-induced LTP was also examined in a separate set of slices, using
596 transient application of the potassium channel blocker tetraethylammonium, applied
597 after completion of a tetanus-induced LTP experiment. As expected,

Medawar et al 2018 - Revision

598 tetraethylammonium application resulted in an initial reduction in the field potential,
599 followed by a long-lasting increase after wash-out. The magnitude of the
600 tetraethylammonium-induced LTP was unchanged in slices of TASTPM compared to
601 wild type animals (data not shown). This confirms that, despite deficits in tetanus-
602 induced LTP, TASTPM are capable of expressing LTP under other induction protocols.
603

604 The deficit in tetanus-induced LTP was maintained at 12 and 18 months of age (Fig 4e).
605

606 Synaptic plasticity in TAS and TPM mice

607 The induction of LTP was also examined in 24 month old single mutant mice (Fig 4f-h).
608 In age-matched wild type mice, LTP magnitude was similar to that observed at younger
609 ages. In the APP_{Swe} TAS mice, the magnitude of LTP was smaller than wild type mice (Fig
610 4f). In contrast, in the PSEN1_{M146V} TPM mice, the magnitude of LTP was greater (Fig 4g).
611 There was an overall significance between genotypes by one-way ANOVA ($p < 0.05$; Fig
612 4h, Fisher LSD *post hoc* tests versus wild type $p = 0.1$ for TAS and $p = 0.05$ for TPM).
613

614 *Cognition and behaviour*

615 TASTPM mice show rigidity in hippocampus-dependent learning

616 The hippocampus-dependent forced-alternation T-maze task was used to assess
617 cognition in the TASTPM mice at three ages (Fig 5): 4 months, which corresponds to the
618 first appearance of A β plaques (Fig 1) and where tetanus induced LTP was first impaired
619 (Fig 4); 8 months, a moderate plaque load and 12 months, a heavy plaque load. Due to
620 availability of animals, in this set of experiments, the 4-month-old group was run as
621 three cohorts (no significant difference between the cohorts); while the 8- and 12-
622 month-old group were a single cohort that underwent repeat training in a longitudinal
623 study. It should be noted that at both 4 and 8 months of age, a subset of TASTPM mice
624 did not complete the task in the required time and these mice were not included in the
625 final results (1 of 16 mice at 4 months of age and 3 of 13 mice at 8 months of age).
626

627 At 4 months of age, both genotypes started training at similar levels of performance and
628 improved over the training period (Fig 5a, two-way ANOVA, main effect of 5 block
629 training period, $p = 0.01$). However, TASTPM performed significantly worse than wild
630 type mice overall (main effect of genotype, $p < 0.003$), and there was no significant

Medawar et al 2018 - Revision

631 interaction between training block and genotype. Interestingly in Block 6, after 2 days
632 without training, the two groups came together with almost identical performance at
633 90% correct choices (Fig 5a). When extra delays (2-6 minutes) were then added
634 between the sample and choice runs a slight decrement in performance occurred, as
635 expected, but there was no difference between genotypes (Fig 5b). In terms of the
636 behaviour within the trials it was notable that on both the sample and choice runs the
637 TASTPM mice showed considerably longer response times. In the case of the choice run,
638 this may have influenced the result, especially the apparent impairment during the
639 training period, as the time that memory needed to be retained was more than doubled
640 (Fig 5c).

641
642 At 8 months of age, TASTPM performed similarly to wild type mice, improving over the
643 training period (two-way ANOVA, main effect of training period ($p < 0.0001$). When the
644 same mice that were run at 8 months were retested at 12 months of age, wild types had,
645 as expected, returned to the baseline response of approximately 75% correct and again
646 improved from ~75% to ~90% during the training period. Unexpectedly however,
647 TASTPM appeared to have retained their previous training, starting the training at
648 ~90% and showed no further improvement over the training period. This was reflected
649 in a significant interaction between training period and genotype in a two-way ANOVA
650 ($p < 0.03$, Fig 5a).

651
652 Animals were again challenged further by the introduction of a delay between sample
653 and choice runs (Fig 5c). While at 8 months there was no difference between genotypes,
654 at 12 months of age although TASTPM mice showed a similar decrement with the
655 longest delays their performance with a 2.5 minute delay between sample and choice
656 runs was surprisingly better than their wild type counterparts (two-tailed t-test,
657 $p < 0.05$).

658
659 Another interesting difference between the 12-month mice and the younger groups was
660 that the response time for the choice run for TASTPM mice at 12 months was rapid and
661 no different from the wild type mice (Fig 5c). (Note, at this age the mice also always
662 completed the task in the required time.) In contrast, as described for 4 months above,
663 the 8-month-old TASTPM mice showed a considerable delay to respond. However,

Medawar et al 2018 - Revision

664 despite this delay again increasing the time that memory needed to be retained, the 8
665 months mice showed no decrement in correct choices.

666
667 These failures and delays to respond may be interesting in terms of early behavioural
668 changes and may also suggest different levels of anxiety.

669
670 TASTPM mice show decreased activity and increased anxiety-related behaviour
671 compared to wild type mice.

672 In the light of the behavioural differences seen in the T-maze trials, locomotor activity
673 and anxiety were assessed using a battery of tests. First, mice were placed in an open
674 field (Fig 6a). TASTPM mice had shorter total path lengths than their wild type
675 counterparts at all ages (Fig. 6ai; two-way ANOVA, main effect of genotype, $p < 0.0001$; no
676 interaction between age and genotype). Furthermore, TASTPM mice spent more time in
677 the peripheral than central area (Fig. 6aii; two-way ANOVA, main effect of genotype,
678 $p < 0.0005$; main effect of age, $p < 0.0001$).

679
680 Secondly, at 8 months of age, TASTPM mice spend more time in the closed than open
681 arms of an elevated plus maze (two-way ANOVA interaction between age and genotype
682 $p < 0.05$); at 4 and 12 months of age this difference was not evident (Fig. 6b).

683
684 Finally, at 4 and 8 months of age, TASTPM mice spent more time in the closed
685 compartment of a light/dark box (12 months not tested). There was a significant
686 interaction between age and genotype (Fig. 6c; $p < 0.05$).

687
688 Overall, these data indicate an increased level of anxiety in TASTPM mice from early
689 stages of plaque development especially at earlier ages.

690 **Discussion**

691 *Pathology and microglia*

692 Proliferation of microglia, particularly clustering around plaques, has been repeatedly
693 reported in Alzheimer's disease, both in the human condition and in mouse models.^[21-23]
694 Moreover we have previously reported a close correlation between plaque load and a
695 microglial coexpression module in TASTPM mice. This reveals not only changes in
696 expression of the gene for the phagocytic protein CD68, tested with
697 immunohistochemistry in the present study but also even greater changes in *Trem2*
698 expression,^[10] a gene shown in humans to be important in Alzheimer's disease in
699 GWAS.^[24, 25] However, here we show increased density of microglia, even before plaques
700 can be detected in this mouse model. This finding required immunohistochemistry and
701 cell counts as the gene expression changes of such specific microglial genes would only
702 be apparent in whole tissue analysis with very large changes, such as occurs in later
703 stages. In the light of previous reports,^[21-23] proliferation seems the most likely
704 explanation of the increased density, although other causes such as increased survival of
705 microglia or migration into the hippocampus, are possible. The triggering of microglial
706 proliferation may be due to soluble A β in the wider neuropil, as seem to be the case for
707 the earliest synaptic changes.^[16] Alternatively, it is possible that initial seeds of plaques
708 are already present at this early stage but are too small to detect, being below the
709 detection threshold set here (<10 μm^2).

710
711 In either case, the question arises as to how plaque development then continues and
712 how this relates to increased microglial numbers and development of a reactive
713 phagocytic phenotype. Once plaques are seeded at these early stages, the ongoing
714 deposition may primarily contribute either to the growth of plaques or to the seeding of
715 new plaques. It is also possible that large plaques are not the result of smaller plaques
716 growing but rather due to the fusion of smaller plaques. Here we observe that the
717 smallest plaques initially increase in number, almost doubling each month. This rate
718 continues to increase, albeit not quite so rapidly, at least until about 14 months of age
719 when the number of plaques plateaus. This suggests that small plaques are seeded
720 throughout the ages tested and gradually grow to form the larger plaques. Presumably
721 the rapid increase in the seeding of plaques during the early stages relates to the rapid
722 increase in A β levels at this stage that we have previously reported.^[16] The plateauing of

Medawar et al 2018 - Revision

723 density of smaller plaques may also reflect them being gradually being engulfed as the
724 larger plaques spread and thus they are no longer seen as separate entities. This is
725 strongly suggested by the appearance of brighter spots of A β in the halo around some of
726 the larger plaques as can be seen in Fig 1a from 10 months onwards.

727

728 As plaques form, we have previously shown a very strong correlation with microglial
729 gene expression.^[10] This encompasses both proliferation and activation of microglia.

730 While there are more microglia very early in these A β mice, their phagocytic phenotype
731 appears later and seems only to be triggered once the larger plaques of >500 μm^2

732 develop. However, it is important to note that a step up in the density of total and CD68

733 positive microglia also occur at this stage in the wild type mice. Although the number of

734 microglia and their activation state remains higher in the TASTPM mice the similarity in

735 the timing of this later stage in both genotypes suggests that this has a strong age-

736 related component rather than being purely dependent on the presence of plaques.

737 However, it is also interesting to note that in the homozygous TASTPM, which develop

738 plaques earlier but plaque load plateaus at the same level as the hemizygous mice, the

739 density of total microglia and CD68 positive microglia is higher than in hemizygotes.

740 Furthermore, the absence of a microglial phenotype in the TPM mice, while the TAS mice

741 show a similar phenotype excludes a direct effect of the mutant presenilin on microglial

742 function.

743

744 As has been previously shown in TASTPM^[10] and other transgenic mice (for example,

745 see reference 22), the microglia are strongly attracted to and cluster tightly around the

746 plaques as they grow. The question arises as to what the microglia are actually doing in

747 the A β mice. The assumption previously has been that they are removing or limiting

748 expansion of plaques.^[22] Conversely, it has been repeatedly reported that removal of

749 microglia by blocking CSF1R has no effect on plaque load,^[26-28] although a role for

750 microglia in initial plaque deposition has been suggested,^[29] which may be related to the

751 initial early rise in microglia numbers, even preceding detection of plaques. It is,

752 however, clear in the TASTPM mice that, since plaques continue to grow in both size and

753 number in parallel to rapid microglial proliferation, it does not seem that microglia are

754 very effective at removing A β . Recently interesting evidence has been presented that A β

755 stimulates microglia to phagocytose synapses in a complement dependent manner at

Medawar et al 2018 - Revision

756 early stages of plaque development in J20 ($APP_{Swe/Ind}$) mice^[30] leading to the hypothesis
757 that microglia are causing early synaptic damage. We put forward an alternative
758 hypothesis that the microglia are rather removing spines and boutons damaged by the
759 high levels of soluble A β in or near the plaques and that this may represent a protective
760 function, avoiding further damage to the dendrites and axons affected and hence
761 protecting network function. This is further supported by the observation that as
762 plaques grow synaptic loss is concentrated near to the plaques and the loss decreases
763 further from plaques.^[31, 32]

764
765 *Synaptic transmission*
766 At 8 months of age the synaptic changes observed are almost identical to those we have
767 previously reported at 4 months, with no change in miniature currents but a complete
768 loss of spontaneous activity and an increase in release probability of glutamate.
769 Particularly at early stages, the plaque load in terms of the percentage tissue coverage is
770 very low and so very few of the synapses recorded would be close to a plaque. Moreover,
771 the observation that the change in paired-pulse ratio is similar despite a rising plaque
772 load also suggests that the plaques themselves are unlikely to be causing this effect.
773 Hence, this is presumably the result of very low levels of soluble A β throughout the
774 tissue. Increased release probability has been reported to be the physiological effect of
775 A β release in wild type rats.^[5] As the plaque load increases and larger plaques start to
776 appear, additional changes become evident. At 12 months, although the evoked release
777 probability is still similarly affected, being higher in the transgenic mice than the wild
778 type mice, there is also a reduction in the frequency of miniature EPSCs. The simplest
779 interpretations of loss of miniature frequency is either a loss of functional synapses or a
780 decreased release probability (see reference 33 for review). As we have demonstrated
781 that release probability is increased, this suggests that there is a loss synapses is the
782 likely explanation. In and around the plaques soluble and insoluble A β will be in
783 equilibrium and with increased plaque coverage with age, at least some of the synapses
784 will be directly affected by the high local concentration of A β in the close vicinity of a
785 plaque which could lead to this loss. Note that unlike evoked currents, miniature
786 synaptic currents can originate from any synapse in the tissue and hence some will be
787 physically near plaques. The increasing effect as the plaque load rises, supports this
788 hypothesis. This is again consistent with the observation that synaptic loss occurs with

Medawar et al 2018 - Revision

821 In concert with (or alternatively to) the direct physiological effects of low levels of A β ,
822 the early increase in LTP magnitude we report could be an interaction with the mutant
823 presenilin 1. Expression of both normal and mutant presenilin 1 has direct effects on
824 synaptic transmission and plasticity. For example, the A246E mutation leads to
825 increased LTP magnitude at young ages,^[38, 39] while the L286V mutation increases LTP
826 magnitude at young ages but decreases at older (14 month) ages.^[40] Here we show that
827 the M146V mutation increases the magnitude of LTP at 24 months of age, which could
828 be the underlying mechanism of the initial increased LTP observed in the TASTPM, until
829 the later A β effects become dominant, decrementing the LTP.

830
831 Interestingly when theta burst stimulation was used for induction, during which the
832 readily-releasable pool would have a chance to replenish, there was no significant deficit
833 in LTP at 4 months. However, under these conditions at 2 months, we see a decrease in
834 paired-pulse ratio following induction of LTP that remains throughout the experiment,
835 indicating an increase in release probability. As outline above, the physiological effect of
836 A β is to increase release probability, and so this suggests that the theta rhythm itself
837 may be causing local release of A β at the stimulated synapses. Despite this apparent
838 presynaptic increase in transmission, the magnitude of LTP remains unaltered, raising
839 the possibility of a postsynaptic decrease balancing this effect. However, when TEA was
840 applied to slices, resulting in a wide-spread depolarisation and thus release of all
841 neurotransmitter vesicles (excitatory, inhibitory and modulatory), LTP was induced
842 similarly to wild types confirming that some forms of long-term plasticity remain intact.
843 In our hands, the locus of expression of LTP, induced by tetanus, tends to have a
844 presynaptic component in both genotypes, indicated by a change in paired-pulse profile
845 following induction.

846
847 *Behaviour*

848 In this study, TASTPM mice showed no measurable cognitive deficits at any age, despite
849 a substantial plaque load.

850
851 There were, however, clear differences in motor activity and anxiety related behaviours.
852 The TASTPM mice were slower to perform the T-maze task than the wild type mice or
853 failed to do so altogether. Furthermore, in other tests, decreased activity and increased

Medawar et al 2018 - Revision

854 anxiety were evident. Although not specifically measured, the TASTPM mice are also
855 more aggressive than wild type mice.^[41]

856

857 The improved retention of learning in TASTPM mice, requiring no repeat training when
858 the same mice were tested twice at 8 and 12 months, may appear counterintuitive.

859 However, similar outcomes in hippocampal learning have been reported in TASTPM
860 mice at around 4 months, using a contextual fear conditioning regime. While mice were
861 unimpaired in learning the task in these previous reports, they failed to extinguish their
862 learnt fear behaviour when conditioning was reversed.^[13, 14, 42] In the present study, the
863 difference was additionally noted, with the TASTPM mice also making more correct
864 choices than the wild type mice when a delay between runs was introduced.

865

866 The subtlety of the cognitive changes reported here in the TASTPM mouse, even at
867 stages where a heavy plaque load is present, is consistent with previous findings.^[13-15, 42]
868 Even when other A β models are considered, cognitive deficits are limited and, where
869 present, it is unclear how they truly translate to the human disease (for reviews, see
870 references 43, 44). Moreover, this is consistent with the human condition, where, at the
871 time of diagnosis, when cognitive deficits are first being detected, there is already a
872 substantial reduction in hippocampal volume of up to 20%,^[45] whereas there is no
873 apparent neuronal loss in TASTPM mice. Furthermore, in humans, cognitive decline
874 correlates well with Tau PET markers and less with A β load.^[46] Given that A β mouse
875 models are not a complete model of AD, i.e. lacking Tau tangle formation and
876 neurodegeneration, which more faithfully correlate with cognitive decline, they should
877 be considered as models of the preclinical disease, when A β is first deposited.

878

879 Here we bring together the progression of pathology, microglia, synaptic transmission
880 and other functional changes in a preclinical mouse model of AD. In a following paper we
881 compare these results in mice with only plaques and no neurofibrillary tangles to a
882 transgenic mouse model of later stage dementia in which neurofibrillary tangles occur
883 without plaques.^[47]

884

885 From the present study we conclude that the earliest effects of A β on synaptic
886 transmission are probably due to very low levels of soluble A β in the volume of the

Medawar et al 2018 - Revision

887 tissue, rather than being directly related to plaques. At this early stage plaques are
888 extremely small and sparse so that they would impinge directly on very few synapses.
889 However, while wide-spread soluble A β may also influence early microglial changes
890 these may well be influenced by the earliest seeding of plaques. Later changes most
891 probably relate to the increasing numbers of larger plaques with the cloud of high-level
892 soluble A β surrounding them impinging on a, still limited, but much greater area. The
893 direct effects of this localised high concentration of soluble A β include loss of active
894 synapses and activation of microglia, likely involved in clearing damaged synapses near
895 or within plaques via phagocytosis and thus preventing wider damage to the affected
896 axons and dendrites. While seeding of new plaques seems to continue throughout the
897 development of plaque pathology, it is only once large plaques are present that these
898 latter changes occur. Moreover, the lack of cognitive deficits is similar to the human
899 situation prior to the build-up of neurofibrillary tangles and neurodegeneration and thus
900 suggests that TASTPM represent a good model of the prodromal phase of the disease.

Medawar et al 2018 - Revision

901 **Data sharing**

902 The datasets used and/or analysed during the current study are available from the
903 corresponding author on reasonable request.

904

905 **Acknowledgements**

906 The authors would like to thank Rivka Steinberg and Stuart Martin for providing
907 genotyping services; Ken Smith, Roshni Desai and Tammaryn Lashley for histological
908 advice; and the Maria Fitzgerald/Steve Hunt laboratories for use of equipment.

909

910 **Funding**

911 GlaxoSmithKline (FAE); BBSRC Case studentship with GSK to PH (FAE); UCL
912 International Studentship to WL (FAE); ARUK and UCL ARUK Network (FAE, DMC, DAS);
913 MRC (FAE); BBSRC for LM (FC)

914 A material transfer agreement between GlaxoSmithKline and UCL for use of the TASTPM
915 mice and agreement for the types of experiment was in place prior to experimental
916 design as well as agreement to include GSK authors. GlaxoSmithKline were not involved
917 directly with the design of the experiments. GlaxoSmithKline (JCR) have read and
918 approved the submitted form of the manuscript. No further input was received from
919 funding sources.

920

921 **Conflicts of Interest**

922 JCR was employed by GlaxoSmithKline during the duration of the experiments
923 performed here in. No further conflicts of interests declared.

924

925 **Authors' contributions**

926 EM performed the histological staining and counting of microglia and provided feedback
927 on draft manuscript. TB carried out behavioural experiments and analysis and
928 comments on draft manuscript. WL performed the LTP experiments at 12 and 18
929 months of age and comments on draft manuscript. TH performed LTP and behavioural

Medawar et al 2018 - Revision

930 experiments at 4 months of age. PH carried out the chemical LTP experiments and
931 comments on draft manuscript. OTJ performed patch clamp experiments for IPSCs at 4
932 months of age. KY performed the LTP experiments at 24 months. LM provided training
933 and supervision of all behavioural experiments. FM performed LTP experiments at 2 and
934 4 months of age. MANS performed behavioural experiments at 4 and 8 months of age. GB
935 carried out histological staining and quantification of plaques. RW performed the
936 microglial histology and counting for the TPM mice. JCR developed the mouse model and
937 comments on the draft manuscript. FC designed and supervised the behavioural
938 experiments and provided comments on the draft manuscript. DAS supervised the
939 histological experiments and commented on draft manuscript. DMC supervised all
940 experiments, performed electrophysiological recordings, wrote first draft of the
941 manuscript, performed all statistical analyses, prepared figures, edited and finalised
942 manuscript. FAE obtained funding, designed experiments, edited and finalised
943 manuscript. All authors read and approved the final manuscript.

944 **References**

- 945 1. Cuyvers E, Sleegers K. Genetic variations underlying Alzheimer's disease:
946 evidence from genome-wide association studies and beyond. *Lancet Neurol* 2016;**15**:
947 857-68. DOI:10.1016/S1474-4422(16)00127-7.
- 948 2. Hardy J, Allsop D. Amyloid deposition as the central event in the aetiology of
949 Alzheimer's disease. *Trends in Pharmacological Sciences* 1991;**12**: 383-8.
- 950 3. Blennow K, Mattsson N, Scholl M, Hansson O, Zetterberg H. Amyloid biomarkers
951 in Alzheimer's disease. *Trends Pharmacol Sci* 2015;**36**: 297-309.
952 DOI:10.1016/j.tips.2015.03.002.
- 953 4. Lewczuk P, Matzen A, Blennow K, et al. Cerebrospinal Fluid Abeta42/40
954 Corresponds Better than Abeta42 to Amyloid PET in Alzheimer's Disease. *J Alzheimers*
955 *Dis* 2017;**55**: 813-22. 10.3233/JAD-160722.
- 956 5. Abramov E, Dolev I, Fogel H, Ciccotosto GD, Ruff E, Slutsky I. Amyloid-beta as a
957 positive endogenous regulator of release probability at hippocampal synapses. *Nat*
958 *Neurosci* 2009;**12**: 1567-76. DOI:10.1038/nn.2433.
- 959 6. Dolev I, Fogel H, Milshtein H, et al. Spike bursts increase amyloid-beta 40/42 ratio
960 by inducing a presenilin-1 conformational change. *Nat Neurosci* 2013;**16**: 587-95.
961 DOI:10.1038/nn.3376.
- 962 7. Iaccarino HF, Singer AC, Martorell AJ, et al. Gamma frequency entrainment
963 attenuates amyloid load and modifies microglia. *Nature* 2016;**540**: 230-5.
964 DOI:10.1038/nature20587.
- 965 8. Verret L, Mann EO, Hang GB, et al. Inhibitory interneuron deficit links altered
966 network activity and cognitive dysfunction in Alzheimer model. *Cell* 2012;**149**: 708-21.
967 10.1016/j.cell.2012.02.046.
- 968 9. Selkoe DJ, Hardy J. The amyloid hypothesis of Alzheimer's disease at 25 years.
969 *EMBO Mol Med* 2016;**8**: 595-608. DOI:10.15252/emmm.201606210.
- 970 10. Matarin M, Salih DA, Yasvoina M, et al. A genome-wide gene-expression analysis
971 and database in transgenic mice during development of amyloid or tau pathology. *Cell*
972 *Rep* 2015;**10**: 633-44. DOI:10.1016/j.celrep.2014.12.041.
- 973 11. Howlett DR, Bowler K, Soden PE, et al. Abeta deposition and related pathology in
974 an APP x PS1 transgenic mouse model of Alzheimer's disease. *Histol Histopathol*
975 2008;**23**: 67-76. DOI:10.14670/HH-23.67.
- 976 12. He Z, Guo JL, McBride JD, et al. Amyloid-beta plaques enhance Alzheimer's brain
977 tau-seeded pathologies by facilitating neuritic plaque tau aggregation. *Nat Med* 2018;**24**:
978 29-38. DOI:10.1038/nm.4443.
- 979 13. Rattray I, Scullion GA, Soulby A, Kendall DA, Pardon MC. The occurrence of a
980 deficit in contextual fear extinction in adult amyloid-over-expressing TASTPM mice is
981 independent of the strength of conditioning but can be prevented by mild novel cage
982 stress. *Behav Brain Res* 2009;**200**: 83-90. DOI:10.1016/j.bbr.2008.12.037.
- 983 14. Rattray I, Pitiot A, Lowe J, et al. Novel cage stress alters remote contextual fear
984 extinction and regional T2 magnetic resonance relaxation times in TASTPM mice
985 overexpressing amyloid. *J Alzheimers Dis* 2010;**20**: 1049-68. DOI:10.3233/JAD-2010-
986 091354.
- 987 15. Howlett DR, Richardson JC, Austin A, et al. Cognitive correlates of Abeta
988 deposition in male and female mice bearing amyloid precursor protein and presenilin-1
989 mutant transgenes. *Brain Res* 2004;**1017**: 130-6. DOI:10.1016/j.brainres.2004.05.029.
- 990 16. Cummings DM, Liu W, Portelius E, et al. First effects of rising amyloid-beta in
991 transgenic mouse brain: synaptic transmission and gene expression. *Brain : a journal of*
992 *neurology* 2015;**138**: 1992-2004. DOI:10.1093/brain/awv127.

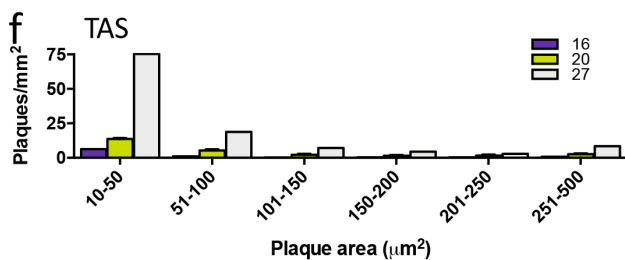
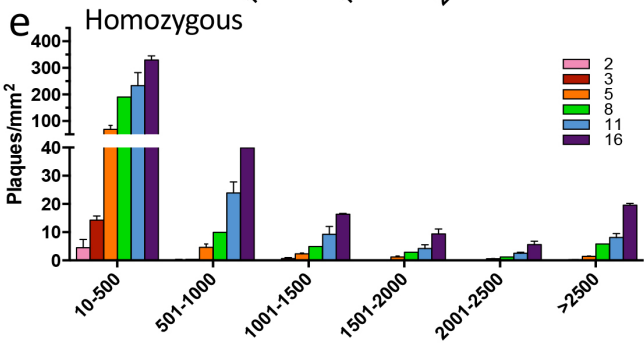
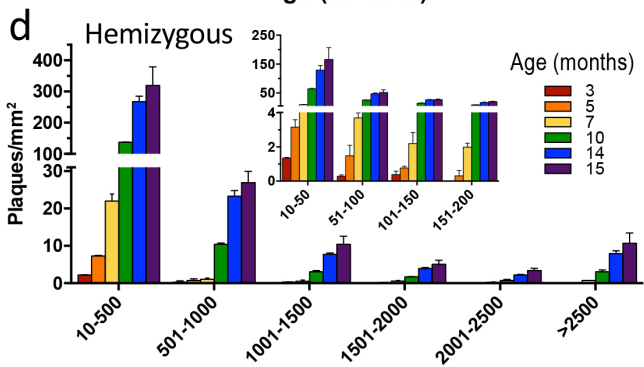
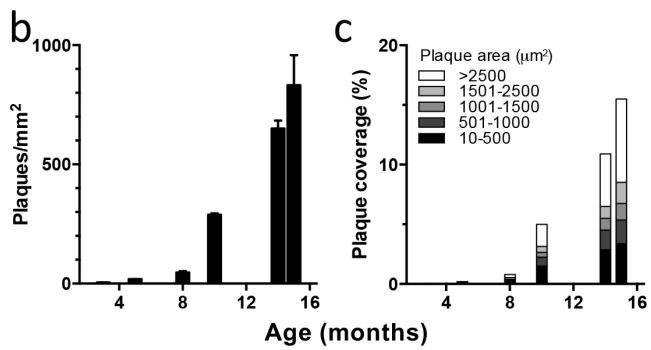
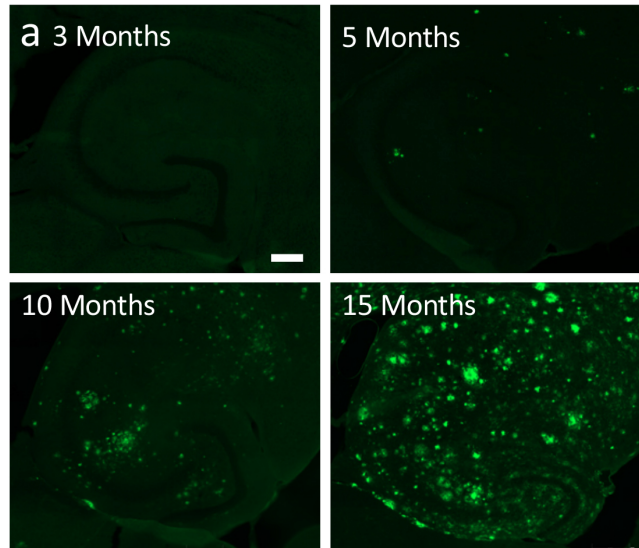
Medawar et al 2018 - Revision

- 993 17. Richardson JC, Kendal CE, Anderson R, et al. Ultrastructural and behavioural
994 changes precede amyloid deposition in a transgenic model of Alzheimer's disease.
995 *Neuroscience* 2003;**122**: 213-28. 10.1016/S0306-4522(03)00389-0.
- 996 18. Cacucci F, Yi M, Wills TJ, Chapman P, O'Keefe J. Place cell firing correlates with
997 memory deficits and amyloid plaque burden in Tg2576 Alzheimer mouse model. *Proc*
998 *Natl Acad Sci U S A* 2008;**105**: 7863-8. DOI:10.1073/pnas.0802908105.
- 999 19. Packard MG, Introini-Collison I, McGaugh JL. Stria terminalis lesions attenuate
1000 memory enhancement produced by intracaudate nucleus injections of oxotremorine.
1001 *Neurobiol Learn Mem* 1996;**65**: 278-82. 10.1006/nlme.1996.0033.
- 1002 20. Bliss TVP, Collingridge GL, Morris RG. Synaptic plasticity in health and disease:
1003 introduction and overview. *Philos Trans R Soc Lond B Biol Sci* 2014;**369**: 20130129.
1004 DOI:10.1098/rstb.2013.0129.
- 1005 21. Nahum-Levy R, Lipinski D, Shavit S, Benveniste M. Desensitization of NMDA
1006 receptor channels is modulated by glutamate agonists. *Biophysical Journal* 2001;**80**:
1007 2152-66.
- 1008 22. Condello C, Yuan P, Schain A, Grutzendler J. Microglia constitute a barrier that
1009 prevents neurotoxic protofibrillar Aβ42 hotspots around plaques. *Nat Commun*
1010 2015;**6**: 6176. DOI:10.1038/ncomms7176.
- 1011 23. Hong S, Dissing-Olesen L, Stevens B. New insights on the role of microglia in
1012 synaptic pruning in health and disease. *Curr Opin Neurobiol* 2016;**36**: 128-34.
1013 DOI:10.1016/j.conb.2015.12.004.
- 1014 24. Guerreiro R, Wojtas A, Bras J, et al. TREM2 variants in Alzheimer's disease. *N Engl*
1015 *J Med* 2013;**368**: 117-27. 10.1056/NEJMoa1211851.
- 1016 25. Jonsson T, Stefansson H, Steinberg S, et al. Variant of TREM2 associated with the
1017 risk of Alzheimer's disease. *N Engl J Med* 2013;**368**: 107-16. 10.1056/NEJMoa1211103.
- 1018 26. Dagher NN, Najafi AR, Kayala KM, et al. Colony-stimulating factor 1 receptor
1019 inhibition prevents microglial plaque association and improves cognition in 3xTg-AD
1020 mice. *J Neuroinflammation* 2015;**12**: 139. DOI:10.1186/s12974-015-0366-9.
- 1021 27. Spangenberg EE, Lee RJ, Najafi AR, et al. Eliminating microglia in Alzheimer's
1022 mice prevents neuronal loss without modulating amyloid-beta pathology. *Brain : a*
1023 *journal of neurology* 2016;**139**: 1265-81. DOI:10.1093/brain/aww016.
- 1024 28. Olmos-Alonso A, Schettters ST, Sri S, et al. Pharmacological targeting of CSF1R
1025 inhibits microglial proliferation and prevents the progression of Alzheimer's-like
1026 pathology. *Brain : a journal of neurology* 2016;**139**: 891-907. 10.1093/brain/aww379.
- 1027 29. Sosna J, Philipp S, Albay R, 3rd, et al. Early long-term administration of the CSF1R
1028 inhibitor PLX3397 ablates microglia and reduces accumulation of intraneuronal
1029 amyloid, neuritic plaque deposition and pre-fibrillar oligomers in 5XFAD mouse model
1030 of Alzheimer's disease. *Mol Neurodegener* 2018;**13**: 11. DOI:10.1186/s13024-018-0244-
1031 x.
- 1032 30. Hong S, Beja-Glasser VF, Nfonoyim BM, et al. Complement and microglia mediate
1033 early synapse loss in Alzheimer mouse models. *Science* 2016;**352**: 712-6.
1034 DOI:10.1126/science.aad8373.
- 1035 31. Spires TL, Meyer-Luehmann M, Stern EA, et al. Dendritic spine abnormalities in
1036 amyloid precursor protein transgenic mice demonstrated by gene transfer and intravital
1037 multiphoton microscopy. *J Neurosci* 2005;**25**: 7278-87. DOI:10.1523/JNEUROSCI.1879-
1038 05.2005.
- 1039 32. Kirkwood CM, Ciuchta J, Ikonovic MD, et al. Dendritic spine density,
1040 morphology, and fibrillar actin content surrounding amyloid-beta plaques in a mouse
1041 model of amyloid-beta deposition. *J Neuropathol Exp Neurol* 2013;**72**: 791-800.
1042 DOI:10.1097/NEN.0b013e31829ecc89.

Medawar et al 2018 - Revision

- 1043 33. Edwards FA. Anatomy and electrophysiology of fast central synapses lead to a
1044 structural model for long-term potentiation. *Physiological Reviews* 1995;**75**: 759-87.
1045 34. Zhang Y, Li P, Feng J, Wu M. Dysfunction of NMDA receptors in Alzheimer's
1046 disease. *Neurol Sci* 2016;**37**: 1039-47. DOI:10.1007/s10072-016-2546-5.
1047 35. Kamenetz F, Tomita T, Hsieh H, et al. APP processing and synaptic function.
1048 *Neuron* 2003;**37**: 925-37.
1049 36. Cirrito JR, Kang JE, Lee J, et al. Endocytosis is required for synaptic activity-
1050 dependent release of amyloid-beta in vivo. *Neuron* 2008;**58**: 42-51.
1051 DOI:10.1016/j.neuron.2008.02.003.
1052 37. Cirrito JR, Yamada KA, Finn MB, et al. Synaptic activity regulates interstitial fluid
1053 amyloid-beta levels in vivo. *Neuron* 2005;**48**: 913-22.
1054 DOI:10.1016/j.neuron.2005.10.028.
1055 38. Parent A, Linden DJ, Sisodia SS, Borchelt DR. Synaptic transmission and
1056 hippocampal long-term potentiation in transgenic mice expressing FAD-linked
1057 presenilin 1. *Neurobiol Dis* 1999;**6**: 56-62. 10.1006/nbdi.1998.0207.
1058 39. Dewachter I, Ris L, Croes S, et al. Modulation of synaptic plasticity and Tau
1059 phosphorylation by wild-type and mutant presenilin1. *Neurobiology of Aging* 2008;**29**:
1060 639-52.
1061 40. Auffret A, Gautheron V, Repici M, et al. Age-dependent impairment of spine
1062 morphology and synaptic plasticity in hippocampal CA1 neurons of a presenilin 1
1063 transgenic mouse model of Alzheimer's disease. *JNS* 2009;**29**: 10144-52.
1064 41. Pugh PL, Richardson JC, Bate ST, Upton N, Sunter D. Non-cognitive behaviours in
1065 an APP/PS1 transgenic model of Alzheimer's disease. *Behav Brain Res* 2007;**178**: 18-28.
1066 DOI:10.1016/j.bbr.2006.11.044.
1067 42. Pardon MC, Sarmad S, Rattray I, et al. Repeated novel cage exposure-induced
1068 improvement of early Alzheimer's-like cognitive and amyloid changes in TASTPM mice
1069 is unrelated to changes in brain endocannabinoids levels. *Neurobiol Aging* 2009;**30**:
1070 1099-113. DOI:10.1016/j.neurobiolaging.2007.10.002.
1071 43. Foley AM, Ammar ZM, Lee RH, Mitchell CS. Systematic review of the relationship
1072 between amyloid-beta levels and measures of transgenic mouse cognitive deficit in
1073 Alzheimer's disease. *J Alzheimers Dis* 2015;**44**: 787-95. DOI:10.3233/JAD-142208.
1074 44. Kobayashi DT, Chen KS. Behavioral phenotypes of amyloid-based genetically
1075 modified mouse models of Alzheimer's disease. *Genes Brain Behav* 2005;**4**: 173-96.
1076 DOI:10.1111/j.1601-183X.2005.00124.x.
1077 45. Ridha BH, Barnes J, Bartlett JW, et al. Tracking atrophy progression in familial
1078 Alzheimer's disease: a serial MRI study. *Lancet Neurol* 2006;**5**: 828-34.
1079 DOI:10.1016/S1474-4422(06)70550-6.
1080 46. Brier MR, Gordon B, Friedrichsen K, et al. Tau and Abeta imaging, CSF measures,
1081 and cognition in Alzheimer's disease. *Sci Transl Med* 2016;**8**: 338ra66.
1082 DOI:10.1126/scitranslmed.aaf2362.
1083 47. Joel Z, Izquierdo P, Liu W, et al. A TauP301L mouse model of dementia;
1084 development of pathology, synaptic transmission, microglial response and cognition
1085 throughout life. *bioRxiv* 2018;**420398**: DOI:10.1101/420398.
1086

Medawar et al 2018 - Revision

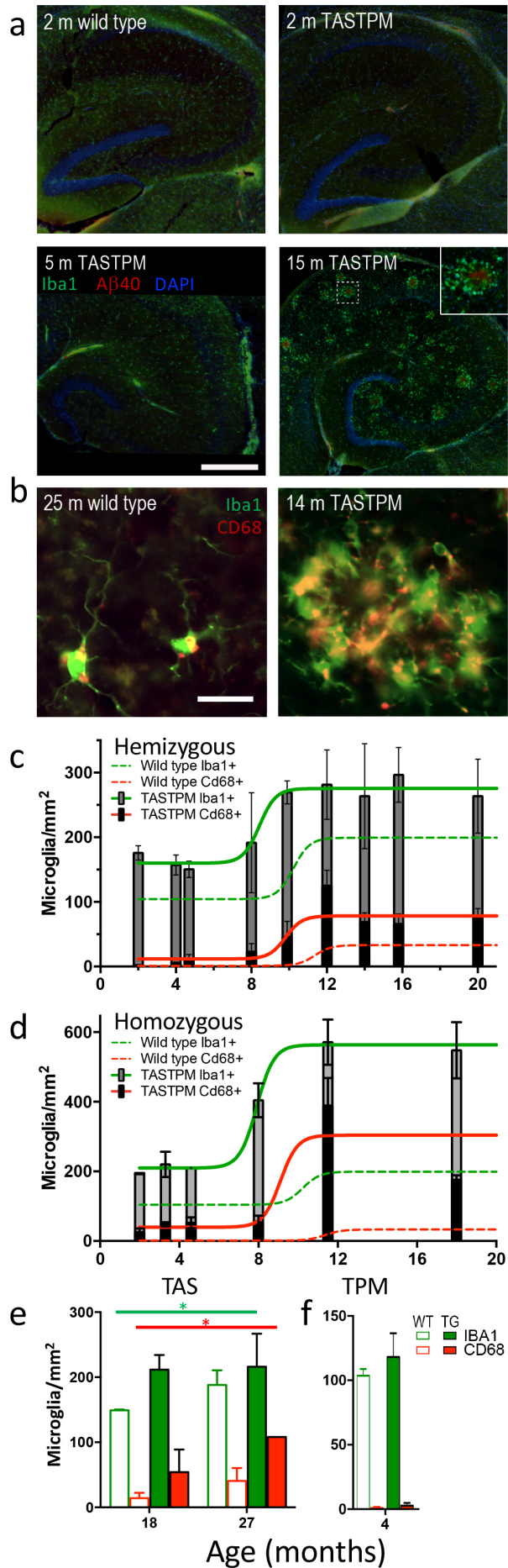


Medawar et al 2018 - Revision

1088 **Figure 1 Plaque development in TASTPM mice**

1089 a) Representative micrographs of A β 40 (green) immunofluorescence in hippocampus
1090 from 3- to 15-month-old hemizygous TASTPM mice. Scale bar 250 μ m. b) Plaque density
1091 measured at different ages in TASTPM mice (n=2-3 animals per age group). c)
1092 Proportion of plaques of indicated sizes contributing to increased percentage coverage
1093 of the hippocampus with increased age. d) Density of plaques within specific size ranges
1094 (as indicated on x-axes) over age (colours as indicated in key). The inset covers smaller
1095 bin sizes for plaques up to 200 μ m². Note the split y-axes. e) Density of homozygous
1096 TASTPM plaques within specific size ranges (as indicated on x-axes) over age (colours as
1097 indicated in key). f) Density of TAS plaques within specific size ranges (as indicated on x-
1098 axes) over age (colours as indicated in key). Note the different x and y-axes in f
1099 compared to d and e, with few plaques and maximum plaque area under 500 μ m². All
1100 data are represented by mean \pm SEM.

Medawar et al 2018 - Revision

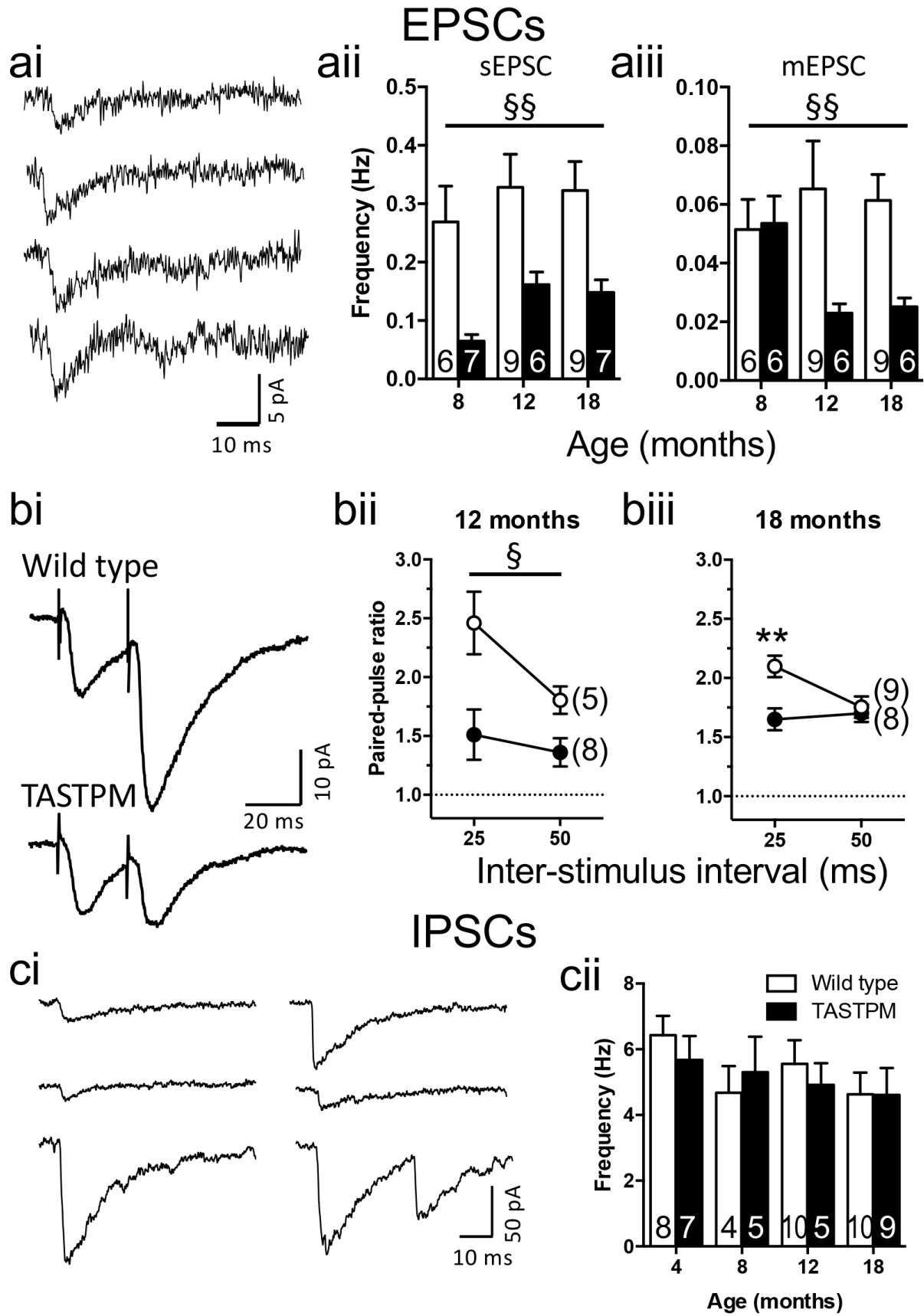


Medawar et al 2018 - Revision

1102 **Figure 2 Microglial proliferation and activation in TASTPM mice**

1103 a) Microglia (Iba1, green) cluster around plaques (A β 1-40, red) in TASTPM mouse
1104 hippocampus (nuclei: DAPI, blue). Scale bar 250 μ m. b) Examples of phagocytic
1105 microglia (CD68, red + Iba1, green; yellow when colocalised) in wild type and TASTPM
1106 hippocampus. Scale bar 25 μ m. c) Total microglial density (Iba1+, full bar height) and
1107 phagocytic microglial (Iba1 + CD68+, black bar) density in hemizygous TASTPM mice
1108 with age. Sigmoidal fits are shown (Iba1 green; CD68 red): unbroken lines, TASTPM;
1109 dashed lines, wild type (only fit shown for wild type). d) Total and phagocytic microglial
1110 densities in homozygous TASTPM mice with age. Sigmoidal fits are shown. e) Total and
1111 phagocytic microglial densities in the APP_{Swe} TAS mice at the ages shown. Significant
1112 main effects of genotype for both IBA1 and CD68 are indicated by *p<0.05. f) Densities of
1113 total microglia and CD68 positive phagocytic microglia in 4 month old PSEN1_{M146V} TPM
1114 microglia. All data are represented by mean \pm SEM.

Medawar et al 2018 - Revision

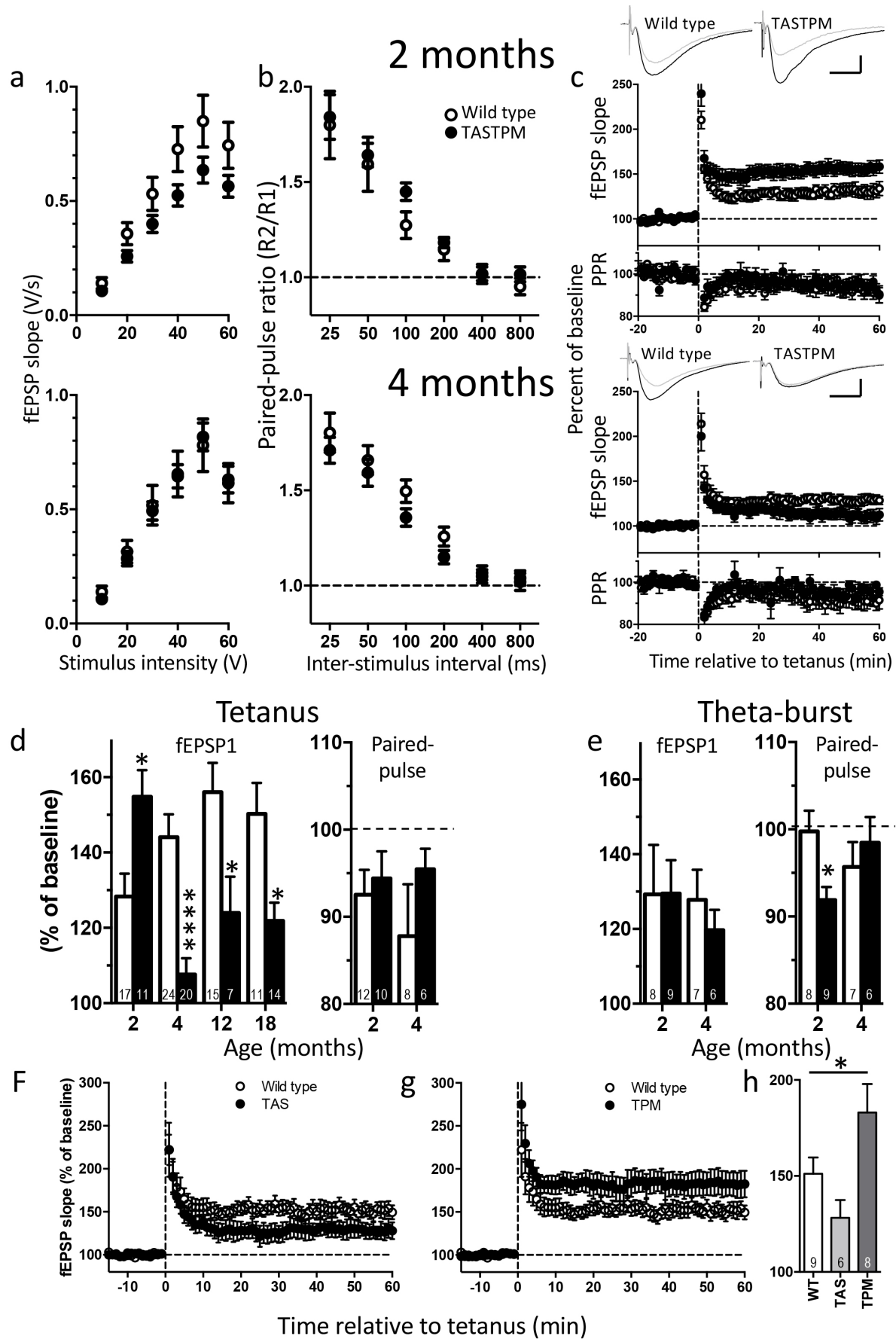


1115

Medawar et al 2018 - Revision

1116 **Figure 3 Excitatory and inhibitory synaptic transmission in TASTPM mice**
1117 ai) Example spontaneous and miniature EPSCs recorded from 18-month-old TASTPM.
1118 aii) Frequency of spontaneous EPSCs. Main effect of genotype by 2-way ANOVA
1119 (p=0.0011). aiii) Frequency of miniature EPSCs. Main effect of genotype by 2-way
1120 ANOVA (p < 0.01) bi) Example responses evoked by paired stimuli. bii) Paired-pulse
1121 ratios from 12-month-old mice. Main-effect of genotype by 2-way ANOVA (p=0.02). (biii)
1122 Paired-pulse ratios from 18-month-old mice. Genotype by inter-stimulus interval
1123 interaction (p<0.05); Sidak post-hoc test is indicated (p=0.002). ci) Example continuous
1124 recordings of spontaneous IPSCs. cii) Spontaneous IPSC frequencies. Sample sizes are
1125 indicated by the numbers within bars or within parentheses. * p<0.05; ** p<0.01. All
1126 data are represented by mean±SEM.

Medawar et al 2018 - Revision

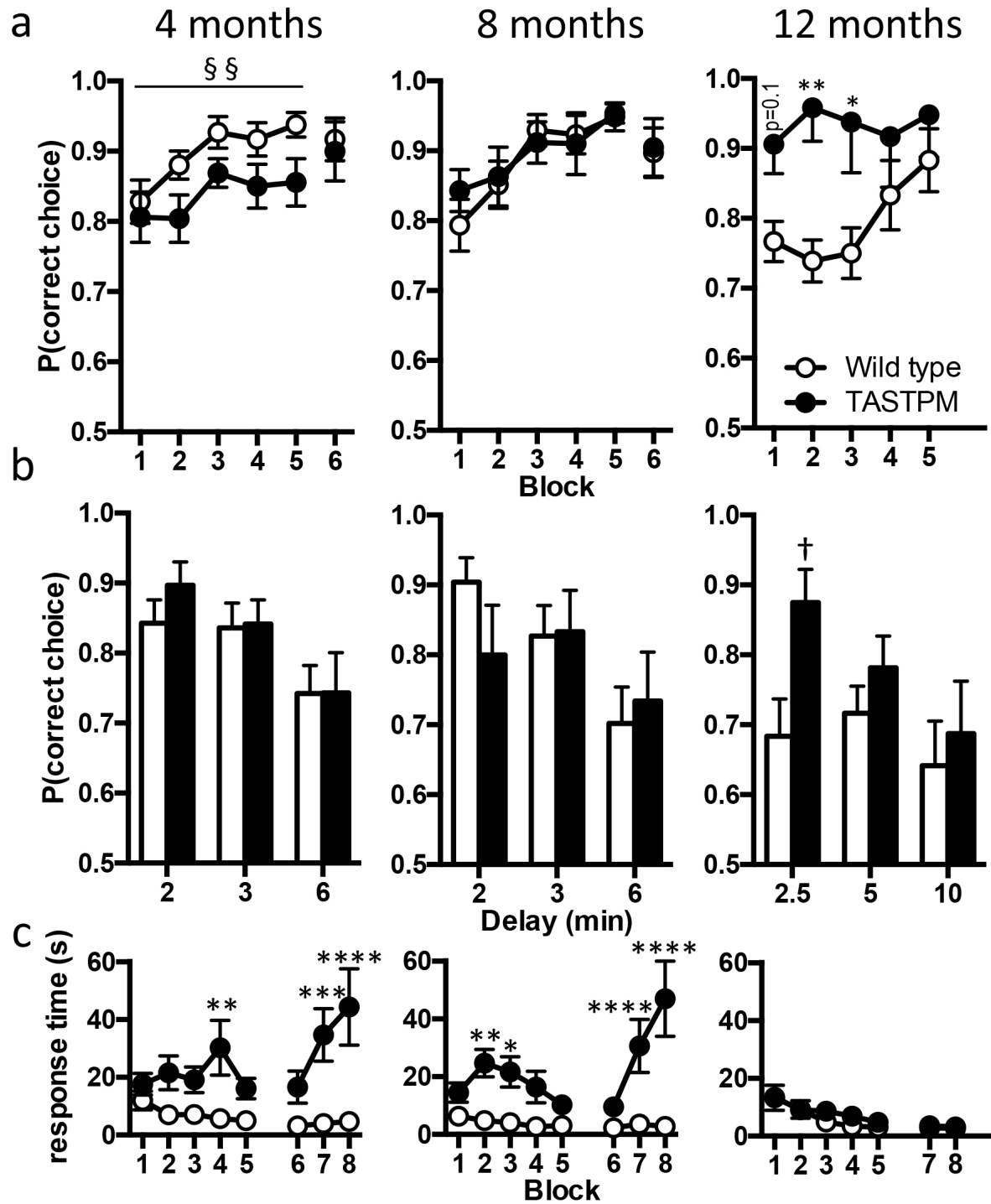


1127

Medawar et al 2018 - Revision

1128 **Figure 4 Field EPSP recordings of synaptic plasticity in TASTPM mice**
1129 a-c) 2 months upper row; 4 months lower row. a) Input-output relationship, b) Paired-
1130 pulse ratio profile and c) Time course of tetanus-induced LTP: fEPSP (upper panels) and
1131 paired-pulse ratio (PPR, lower panels) after induction as a percentage of pre-induction
1132 baseline. Traces are representative fEPSPs from baseline (grey) and the 51-60 minutes
1133 after tetanus (black). Scale bars: 5 ms x 0.5 mV. d) Magnitude of LTP (*left*) induced by
1134 tetanus over 2-18 months of age (number of mice as indicated in each column). Two-
1135 way ANOVA revealed significant age x genotype interaction ($P < 0.0001$). Change in
1136 paired-pulse ratio (*right*) following LTP induction. Both wild type and TASTPM mice
1137 showed a significant decrease in PPR compared to baseline at both ages (paired t-tests
1138 within separate experiments; $p < 0.05$). No significant difference between genotypes
1139 (two-way ANOVA). e) Magnitude of LTP induced by theta-burst stimulation (*left*, no
1140 significant difference between genotypes) and corresponding change in paired-pulse
1141 ratio (*right*; two-way ANOVA age x genotype interaction $p < 0.05$). Sidak post hoc test:
1142 * $P < 0.05$; **** $P < 0.0001$. f) LTP induced by tetanic stimulation in APP_{Swe} TAS mice at 24
1143 months of age. g) LTP induced by tetanic stimulation in PSEN1_{M146V} TPM mice at 24
1144 months. Wild type animals are common to both panels f and g. h) Magnitude of LTP
1145 induced in 24 month old wild type, TAS and TPM mice. 24 month old recordings for all
1146 genotypes were interleaved; significance tested by one-way ANOVA, * $p < 0.05$. All data
1147 are represented by mean \pm SEM.

Medawar et al 2018 - Revision



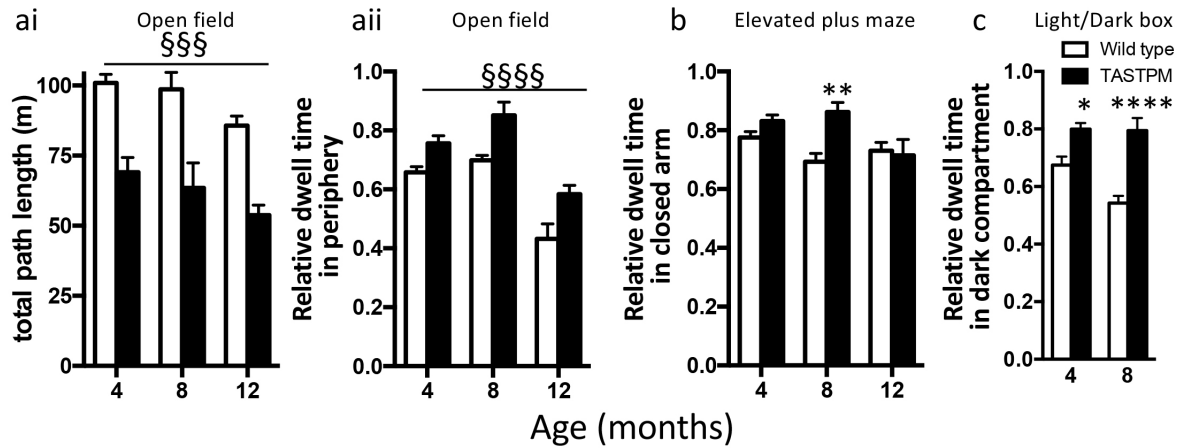
1148

Medawar et al 2018 - Revision

1149 **Figure 5 Hippocampus-dependent T-Maze learning in TASTPM mice**

1150 a-c) Ages as indicated above panel a. a) Probability of mice making a correct choice in
1151 the choice run at 4 months (n=15-16 animals completing the task), 8 months (n=10-13
1152 animals completing the task) and 12 months of age (wild type n=15; TASTPM n=8). At 4
1153 months of age there was a main effect of genotype in a two-way ANOVA (§§ p<0.01).
1154 Note the difference in starting performance at 12 months of age. These are the same
1155 mice tested at 8 months. As expected wild type mice started at around 75% correct
1156 choices and improved with training having, extinguished their previous training.
1157 TASTPM mice unexpectedly started training making correct choices 90% of the time
1158 having retained the previous improved level. Two-way ANOVA interaction between
1159 training block and genotype (p<0.03); Sidak post hoc analyses are indicated by *P<0.05,
1160 **P<0.01. b) The introduction of delays between sample and choice runs revealed no
1161 further differences between genotypes at 4 or 8 months of age, while at 12 months, a
1162 significant effect of genotype was observed with TASTPM mice retaining performance
1163 despite a 2.5 minute delay before the choice run († p<0.05). c) Response time for choice
1164 run at 4 -12 months of age, Sidak post hoc analyses are indicated by *P<0.05, **P<0.01,
1165 ***P<0.001, ****P<0.0001. All data are represented by mean±SEM.

Medawar et al 2018 - Revision



1166

1167

1168 **Figure 6 Open field and tests of anxiety**

1169 a) Open field test. ai) Total path length run over 30 mins. Main effect of genotype by two-
 1170 way ANOVA (\$\$\$ p<0.001). aii) Time spent in peripheral area. Main effect of genotype by
 1171 two-way ANOVA (\$\$\$\$ p<0.0001). b) Elevated plus maze. Relative time in closed arm. c)
 1172 Light/dark box. Relative time spent in dark compartment (12 months not tested.) In b
 1173 and c, Sidak post hoc tests are indicated (two-way ANOVA genotype x age interaction
 1174 P<0.05; * p<0.05; ***p<0.001; **** p<0.0001). All data are represented by mean±SEM.

Medawar et al 2018 - Revision

1175 **Table 1:** *Antibodies used for immunohistochemistry:*

Antibody	Dilution	Source	RRID
IBA1	1:500	Wako (019-19741)	AB_839504
CD68	1:500	BioRad (MCA1957)	AB_322219
A β 1-40	1:300	ThermoFisher (44-136)	AB_2533599

1176